Molecular Passivation of MoO_3: Band Alignment and Protection of Charge Transport Layers in Vacuum-Deposited Perovskite Solar Cells

Daniel Pérez-del-Rey[1], Lidón Gil-Escrig[2], Kassio P.S. Zanoni[1,3], Chris Dreessen[1], Michele Sessolo[1], Pablo P. Boix[1,*], Henk J. Bolink[1,*]

[1]Instituto de Ciencia Molecular, Universidad de Valencia, C/ Catedrático J. Beltrán 2, 46980 Paterna, Spain

[2]Helmholtz-Zentrum Berlin für Materialien und Energie GmbH, Kekuléstraße 5, 12489 Berlin, Germany

[3]Istituto de Física de São Carlos, Universidade de São Paulo, Av. Trab. São Carlense 400, 13566 São Carlos, Brazil

ABSTRACT: Vacuum-deposition of perovskite solar cells can achieve efficiencies rivalling solution-based methods and it allows for more complex device stacks. MoO_3 has been used to enhance carrier extraction to the transparent bottom electrode in a p-i-n configuration, here we show that by inserting an organic charge transport molecule it can also be used on the top of a perovskite absorber in a n-i-p configuration. This strategy enables the first vacuum-deposited perovskite solar cells with metal oxides as charge transporting layers for both electrons and holes leading to power conversion efficiency > 19 %.

1. Introduction

Halide perovskites have a wide range of chemical and physical properties that make them suitable for new generation photovoltaics.[1] These encompass long charge carrier diffusion lengths[2] and high absorption coefficients.[3] Furthermore, their compositional flexibility allows the fine tuning of the photophysical properties.[4,5] The use of perovskites in high efficiency devices requires directing charge carriers to the appropriate electrode. This is generally achieved by placing selective charge transport layers below and above the perovskite layer. Interfaces between the perovskite and the charge extraction material, and between the charge extraction material and the electrodes, are thus crucial for an efficient charge carrier collection.[6] In this aspect, perovskite-based solar cells can have two main device architectures depending on whether the photogenerated holes are extracted through the light incident side and photogenerated electrons extracted through the metal side (p-i-n) or vice versa (n-i-p), just by changing the deposition order of the transport layers.

Vacuum deposition is a widely adopted technique in the industry, with proven scalability capabilities. More interestingly for perovskite optoelectronics, it is a solvent-free process making it more environmentally friendly.[7] Vacuum processing also allows for an accurate control on multiple layers stacks.[8] Vacuum-deposited high efficiency solar cells generally rely on a combination of intrinsic organic materials, as charge selective layers, and doped materials, as charge transport/extraction layers, to ensure that the photogenerated charge carriers are efficiently extracted to an external circuit[9].

Semiconducting metal oxides are widely studied in solution-processed perovskite devices and have also been recently applied as charge transport layers in high efficient vacuum-deposited perovskite solar cells[10]. The use of TiO_2 in n-i-p structure instead of doped C_{60} reduces parasitical absorption and has a positive impact on device stability and material costs.[10] However, the system still relies on organic doped materials as hole transport layer (HTL) in the top contact, with the associated complexity and stability-related issues. Hence, it is important to find metal oxide alternatives that can reduce parasitic absorption in p-i-n devices and can be incorporated to a n-i-p stack without compromising the rest of the deposited layers.

Molybdenum (VI) oxide (MoO_3) has been recurrently employed as hole injection/extraction layers in OLEDs,[11] and in organic, quantum dot and perovskite solar cells,[12,13] due to its very deep work function and low-lying conduction band.[14] MoO_3 has the advantage of creating an optimal ohmic contact with ITO. Its protective effect against moisture when used in this architecture has also been reported.[15] Together with its low parasitic absorption and the possibility of being sublimed, it appears as a good candidate for its use as a hole extraction material in our system. However, the low selectivity of MoO_3 requires it to be used in combination with more selective contacts.

Here, we develop a method to modify the MoO_3 / electron blocking layer interface, obtaining an improved

ohmic contact suitable for p-i-n configuration, yet with the advantage of avoiding any annealing step. In the n-i-p structure, this interfacial modification also acts as a protection layer which prevents MoO_3 diffusion into the underlying layers. As a result, we fabricate the first high efficiency vacuum deposited perovskite solar cell with both charge extraction layers based on metal oxides.

2. Experimental methods

Photolithographically patterned ITO coated glass substrates were purchased from Naranjo Substrates. N4,N4,N4',N4'-tetra([1,1'-biphenyl]-4-yl)-[1,1':4',1'-terphenyl]-4,4'-diamine (TaTm) were provided by Novaled GmbH. TiO_2 nanoparticle suspensions were prepared in IMEC as previously reported.[10] Fullerene (C_{60}) was purchased from sigma Aldrich. PbI_2 was purchased from Tokyo Chemical Industry CO (TCI), while CH_3NH_3I (MAI), MoO_3 and bathocuproine (BCP) were purchased from Lumtec.

ITO prepatterned substrates were cleaned following a standard procedure in which they are cleaned with soap, water, de-ionized water and isopropanol in a sonication bath, followed by UV treatment for 20 min. The TiO_2 dispersion was deposited in air by spin-coating at 3000 rpm for 30 s and annealed at 100 °C for 30 min, leading to a 50–80 nm thick compact layer. For the deposition of the other materials through vacuum deposition, the samples were transferred to a vacuum chamber integrated into a nitrogen-filled glovebox (H_2O and O_2 < 0.1 ppm) and evacuated to a pressure of 10^{-6} mbar. The vacuum chamber is equipped with six temperature-controlled evaporation sources (Creaphys) fitted with ceramic crucibles. The sources were directed upward with an angle of approximately 90° with respect to the bottom of the evaporator. The substrate holder to evaporation sources distance is approximately 20 cm. Three quartz crystal microbalance (QCM) sensors are used: two monitoring the deposition rate of each evaporation source and a third one close to the substrate holder monitoring the total deposition rate. For thickness calibration, we individually sublimed the charge transport materials. A calibration factor was obtained by comparing the thickness inferred from the QCM sensors with that measured with a mechanical profilometer (Ambios XP1). Then, the materials were sublimed at temperatures ranging from 60 ºC to >300 ºC, and the evaporation rate was controlled by separate QCM sensors obtaining precisely the deposited thickness. In general, the deposition rate for TaTm and C60 was 0.5 Å s^{-1} and 0.2-0.3 Å s^{-1} for the thinner BCP, TPBi, CBP and TCTA layers. For the perovskite deposition, MAI and PbI_2 were co-evaporated by measuring the deposition rate of each material in a different sensor and obtaining the total perovskite thickness in a third one, leading to a 590 nm thick perovskite. MoO_3, Ag and Au were evaporated in a second vacuum chamber using aluminum boats as sources by applying currents ranging from 2.0 to 4.5 A. For the solar cell characterization, the J–V characteristics were obtained using a solar simulator by Abet Technologies (model 10500 with an AM1.5G xenon lamp as the light source). Before each measurement, the exact light intensity was determined using a calibrated Si reference diode equipped with an infrared cutoff filter (KG-3, Schott). The J–V curves were recorded between –0.2 and 1.2 V with 0.01 V steps, integrating the signal for 20 ms after a 10 ms delay. This corresponds to a speed of about 0.3 V s^{-1}. The layout used to test the solar cells has four equal areas (0.0651 cm^2, defined as the overlap between the ITO and the top metal contact) and measured through a shadow mask with 0.0264 cm^2 aperture. Absorption spectra were collected using a fiber optics based Avantes Avaspec2048 Spectrometer. The work functions were determined by Kelvin probe measurements using an Ambient Pressure Photoemission Spectroscopy system from KP Technology.

3. Results

In order to evaluate the overall capability of MoO_3 as a hole extraction layer, the following p-i-n configuration was selected as it is similar to a previously tested one with an organic charge extraction material (F6TCNNQ)[9]; ITO/MoO_3 (7 nm)/TaTm (10 nm)/$CH_3NH_3PbI_3$ (590 nm)/C60 (25 nm)/BCP (7 nm)/Ag, as represented in Figure 1.

In Figure 1b and 1c, respectively, the typical current-voltage curves in the dark and under AM1.5G are depicted for three different hole extraction layers. The devices with non-annealed (as deposited) MoO_3 show a high short circuit current density, J_{sc} (21 mA/cm^2) a reasonable open circuit voltage, V_{oc} (1.03V) but a rather poor fill factor, FF (73 %). This may be due to either a low layer conductivity, to an energy level mismatch with the electron blocking material, or to a combination of both. It has been reported that annealing the MoO_3 layer increases the amount of oxygen vacancies and creates gap states, which can contribute to the charge transport through a shift in the Fermi level.[16,17] We also find that an annealing process of the MoO_3 layers for 10 min at 100 ºC in nitrogen leads to an increase in FF and also in J_{sc} and V_{oc} values. This is most likely the result of the work function (WF) closer to the vacuum level, as shown in Figure S1. Despite the higher power conversion efficiencies obtained, the temperature requirement for this annealing step are undesired. Therefore, we also considered an alternative approach to interfacial tuning by adding an interlayer with a lower ionization energy (IE) than the WF of the MoO_3, as was recently reported for similar devices.[18] We used 2,2′,2"-(1,3,5-Benzinetriyl)-tris(1-phenyl-1-H-benzimidazole) (TPBi) in a 2 nm thin interlayer between the un-annealed MoO3 and the hole transport/electron blocking molecule TaTm. These devices have very similar performance as in the device with the annealed MoO_3 (Figure 1). The insertion of this interlayer is confirmed by contact angle measurements and does not lead to additional absorption (Figures S2 and S3).

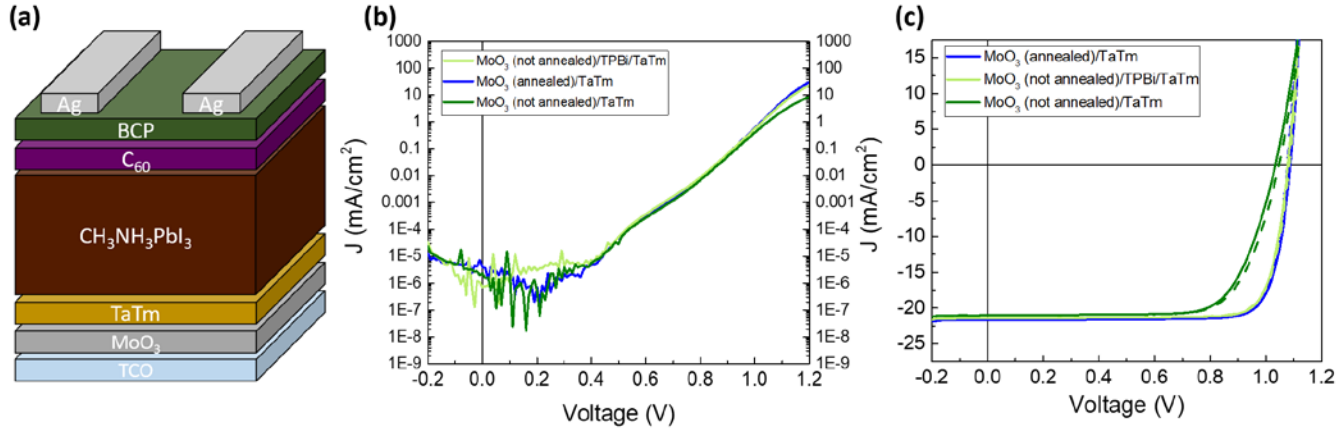

Figure 1. a) Schematic device architecture, b) dark and c) illuminated J-V curves (AM1.5G) of p-i-n devices according to panel a, for three different hole extraction architectures, MoO_3 (not annealed)/TaTm, MoO_3 (annealed)/TaTm and MoO_3 (not annealed)/TPBi/TaTm. Dashed lines in figure c stand for reverse scan.

Table 1: Average solar cell parameters for p-i-n solar cells with the MoO_3 layer at the front contact.

Samples	PCE (%)	V_{oc} (V)	J_{sc} (mA/cm2)	FF (%)
MoO_3 (not annealed)	15.8	1.034	21.0	73.0
MoO_3 (annealed)	19.3	1.077	21.7	82.5
MoO_3 (not annealed)/TPBi	19.0	1.080	21.4	82.0

Some other molecules were also sublimed and evaluated as interlayers in between not annealed MoO_3 and TaTm, namely, TCTA (Tris(4-carbazoyl-9-ylphenyl)amine) and CBP (4,4'-Bis(N-carbazolyl)-1,1'-biphenyl). These molecular layers also improve the device behavior but not to the extent that MoO_3 annealing or TPBi insertion does (figure S4) which is in agreement with a lower difference between their IE (CBP = 6.0 eV and TcTa = 5.7 eV) and the HOMO level of TaTm, as was discussed also in Reference nr 18.

Since the TPBi interlayer enables the use of MoO_3 as hole extraction layer without the need for its annealing, this extraction layer can now be directly implemented in a n-i-p structure with both contacts based on metal oxides. The chosen device structure for the n-i-p devices is TiO_2 (50-80 nm)/C_{60} (10 nm)/$CH_3NH_3PbI_3$ (590 nm)/TaTm (10 nm)/(TPBi 2 nm, optional)/MoO_3 (5 nm)/Au (Figures 2a and 2b).

In Figure 2c, the typical current-voltage curves in the dark and under AM1.5G are depicted for the n-i-p devices with three different hole extraction layers and the parameters are listed in Table 2. The devices with TaTm and the non-annealed (as deposited) MoO_3 show a rather low V_{oc} but a decent FF. This is most likely due to diffusion of MoO_3 into TaTm, as previously reported for various organic materials.[19] While this diffusion of MoO_3 has the potential to improve the band alignment without further annealing, it can also significantly increase recombination losses due to the partial or complete oxidation of the TaTm electron blocking layer. The much higher dark current (hence, high conductivity) observed for the TaTm/MoO_3 containing device compared to the one with the TPBi thin interlayer (see Figure S5a) is in agreement with this hypothesis. Such a reduced electron blocking and hence increased charge recombination would indeed lead to a lower V_{oc} without affecting too much the FF, as we observe. The device with a 2 nm TPBi interlayer in between the TaTm layer and the MoO_3 layer shows very good performance, with high V_{oc}, J_{sc} and FF leading to a power conversion efficiency of almost 19 %. Although, a similarly thin layer of TPBi also improved the performance of the p-i-n devices, it is rather surprising that such a thin layer is preventing the diffusion of MoO_3 into the TaTm layer. Therefore, we also prepared a similar device but now with a slightly thicker TPBi layer of 5 nm. In these devices the V_{oc} is similar to what is observed for the device with a 2 nm layer, but the FF is much worse, indicating a significant extraction barrier due to a strong increase in the series resistance. This seems to indicate that the MoO_3 interacts only with the surface of the TPBi layer, as intrinsic TPBi is a poor hole transporter and undoped TPBi needs to be very thin to effectively tunel holes through. To verify if MoO_3 diffusion and the accompanied reduction in electron blocking behavior can also be

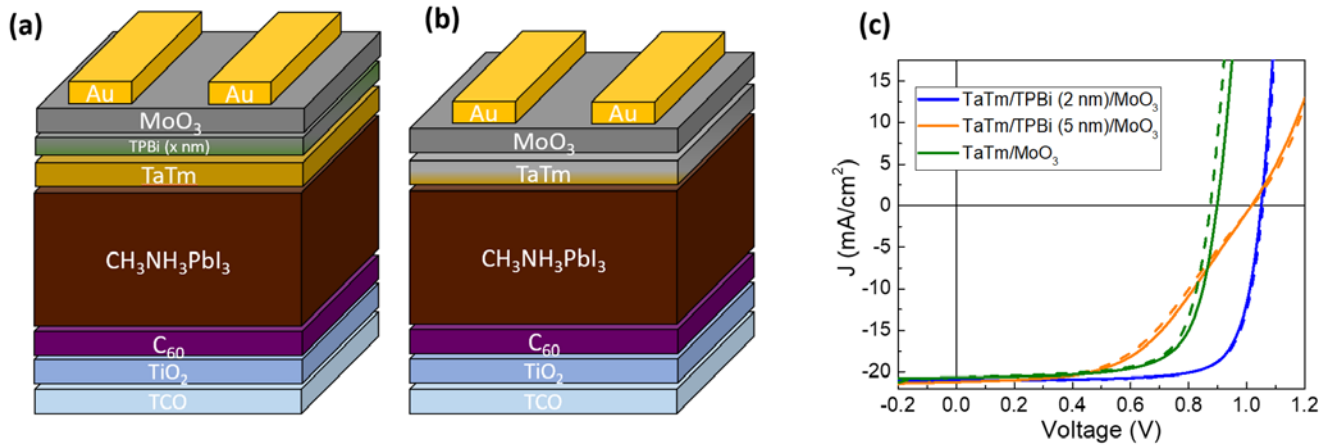

Figure 2. Schematic device architectures of n-i-p devices with (a) and without (b) TPBi interlayer. c) J–V curves under AM1.5G illumination corresponding to devices with 0, 1 and 5 nm thick TPBi interlayer. Dashed lines stand for reverse scan

Table 2: Average PV parameters of n-i-p solar cells with MoO_3 on top of TaTm and on top of TaTm/TPBi.

Sample	PCE (%)	V_{oc} (V)	J_{sc} (mA/cm2)	FF (%)
TaTm/MoO_3	13.0	0.898	20.7	70.0
Tatm/TPBi (2 nm)/MoO_3	18.8	1.084	21.3	81.4
Tatm/TPBi (5 nm)/MoO_3	11.0	1.015	21.2	51.0

reduced by using thicker TaTm layers, such devices were prepared as well. In these solar cells, the V_{OC} recovers, as displayed in Figure S5b. However, the MoO_3 diffusion is a sensitive process difficult to control, and thicker TaTm n-i-p solar cells suffer from poorer reproducibility and larger parasitic absorption. In order to evaluate this TPBi interaction with MoO_3, we substitute TPBi with TCTA. As in the p-i-n devices it leads to similar device performance (Figure S4). However, in the n-i-p configuration devices with a 2 nm thick TCTA interlayer have low V_{oc}'s similar as the TPBi-free devices, which is attributed to the diffusion of MoO_3 into both TCTA and TaTm, increasing recombination and reducing the V_{oc} (Figure S6). The molecular weight of TCTA and TPBI are very similar and therefore is unlikely the reason for the observed difference in device performance. The reactivity of MoO_3 with organic compounds is well-known, particularly with pyridine-like nitrogen atoms with a lone pair such as bipyridine, where the ligand passivates MoO_3 surface and blocks further Mo–oxo bond formation, or with triazole family molecules forming different layered structure.[20,21] TPBi, contains a lone pair which may lead to chemical modification of the MoO_3 surface creating possibly the before mentioned oxygen vacancies that contribute to the charge transport, as other works have shown with pyridine-like nitrogen atoms. [17,20,22] For this reason, a 2nm layer of Bathocuproine (BCP, 2,9-Dimethyl-4,7-diphenyl-1,10-phenanthroline) was also inserted in the n-i-p device stack. The performance of the resulting solar cells is very similar as in the case of the TPBi interlayers (Fig. S6) indicating that there is an interaction between MoO_3 and these pyridine containing molecules that prevents the diffusion of MoO_3.

Considering both the p-i-n and n-i-p results, we hypothesize that TPBi reacts with MoO_3 surface through an electron transfer, facilitating the charge transport. Not only that, but also this TPBi-MoO_3 surface species protects TaTm in the inverted structure from the diffusion of MoO_3 by forming a passivation layer, which makes it possible to use this material in n-i-p configuration without compromising the performance nor reproducibility of the device.

4. Conclusions

In conclusion, the insertion of a thin layer of a wide bandgap conjugated molecule containing pyridine like moieties leads to efficient hole extraction in p-i-n and n-i-p architectures. In part due to the decoupling of the dipole moment and additionally be preventing evaporation damage of MoO3 on the organic charge transporting molecules. The efficient charge extraction and resulting device efficiency in the n-i-p configuration is particularly promising as it can be used in tandem cells and low temperature demanding substrates.

REFERENCES

(1) Xu, W.; Cho, H.; Kim, Y.-H.; Kim, Y.-T.; Wolf, C.; Park, C.-G.; Lee, T.-W. Organometal Halide Perovskite Artificial Synapses. *Adv. Mater.* **2016**, *28* (28), 5916–5922. https://doi.org/10.1002/adma.201506363.

(2) Shi, D.; Adinolfi, V.; Comin, R.; Yuan, M.; Alarousu, E.; Buin, A.; Chen, Y.; Hoogland, S.; Rothenberger, A.; Katsiev, K.; et al. Low Trap-State Density and Long Carrier Diffusion in Organolead Trihalide Perovskite Single Crystals. *Science (80-.).* **2015**, *347* (6221), 519–522. https://doi.org/10.1126/science.aaa2725.

(3) De Wolf, S.; Holovsky, J.; Moon, S.-J.; Löper, P.; Niesen, B.; Ledinsky, M.; Haug, F.-J.; Yum, J.-H.; Ballif, C. Organometallic Halide Perovskites: Sharp Optical Absorption Edge and Its Relation to Photovoltaic Performance. *J. Phys. Chem. Lett.* **2014**, *5* (6), 1035–1039. https://doi.org/10.1021/jz500279b.

(4) Cheetham, A. K.; Rao, C. N. R.; Feller, R. K. Structural Diversity and Chemical Trends in Hybrid Inorganic?Organic Framework Materials. *Chem. Commun.* **2006**, No. 46, 4780. https://doi.org/10.1039/b610264f.

(5) Li, W.; Wang, Z.; Deschler, F.; Gao, S.; Friend, R. H.; Cheetham, A. K. Chemically Diverse and Multifunctional Hybrid Organic-Inorganic Perovskites. *Nat. Rev. Mater.* **2017**, *2* (3), 16099. https://doi.org/10.1038/natrevmats.2016.99.

(6) Fakharuddin, A.; Schmidt-Mende, L.; Garcia-Belmonte, G.; Jose, R.; Mora-Sero, I. Interfaces in Perovskite Solar Cells. *Adv. Energy Mater.* **2017**, *7* (22), 1700623. https://doi.org/10.1002/aenm.201700623.

(7) Ávila, J.; Momblona, C.; Boix, P. P.; Sessolo, M.; Bolink, H. J. Vapor-Deposited Perovskites: The Route to High-Performance Solar Cell Production? *Joule* **2017**, *1* (3), 431–442. https://doi.org/10.1016/j.joule.2017.07.014.

(8) Ávila, J.; Momblona, C.; Boix, P.; Sessolo, M.; Anaya, M.; Lozano, G.; Vandewal, K.; Míguez, H.; Bolink, H. J. High Voltage Vacuum-Deposited CH 3 NH 3 PbI 3 –CH 3 NH 3 PbI 3 Tandem Solar Cells. *Energy Environ. Sci.* **2018**, *11* (11), 3292–3297. https://doi.org/10.1039/C8EE01936C.

(9) Momblona, C.; Gil-Escrig, L. L.; Bandiello, E.; Sessolo, M.; Hutter, E. M.; Lederer, K.; Blochwitz-Nimoth, J. B.-N.; Bolink, H. J.; Sessolo, M.; Lederer, K.; et al. Efficient Vacuum Deposited P-i-n and n-i-p Perovskite Solar Cells Employing Doped Charge Transport Layers. *Energy Environ. Sci.* **2016**, *9* (11), 3456–3463. https://doi.org/10.1039/C6EE02100J.

(10) Pérez-del-Rey, D.; Boix, P. P.; Sessolo, M.; Hadipour, A.; Bolink, H. J. Interfacial Modification for High-Efficiency Vapor-Phase-Deposited Perovskite Solar Cells Based on a Metal Oxide Buffer Layer. *J. Phys. Chem. Lett.* **2018**, *9* (5), 1041–1046. https://doi.org/10.1021/acs.jpclett.7b03361.

(11) You, H.; Dai, Y.; Zhang, Z.; Ma, D. Improved Performances of Organic Light-Emitting Diodes with Metal Oxide as Anode Buffer. *J. Appl. Phys.* **2007**, *101* (2), 26105. https://doi.org/10.1063/1.2430511.

(12) Shrotriya, V.; Li, G.; Yao, Y.; Chu, C.-W.; Yang, Y. Transition Metal Oxides as the Buffer Layer for Polymer Photovoltaic Cells. *Appl. Phys. Lett.* **2006**, *88* (7), 73508. https://doi.org/10.1063/1.2174093.

(13) Gao, J.; Perkins, C. L.; Luther, J. M.; Hanna, M. C.; Chen, H.-Y.; Semonin, O. E.; Nozik, A. J.; Ellingson, R. J.; Beard, M. C. N-Type Transition Metal Oxide as a Hole Extraction Layer in PbS Quantum Dot Solar Cells. *Nano Lett.* **2011**, *11* (8), 3263–3266. https://doi.org/10.1021/nl2015729.

(14) Meyer, J.; Hamwi, S.; Kröger, M.; Kowalsky, W.; Riedl, T.; Kahn, A. Transition Metal Oxides for Organic Electronics: Energetics, Device Physics and Applications. *Adv. Mater.* **2012**, *24* (40), 5408–5427. https://doi.org/10.1002/adma.201201630.

(15) Sanehira, E. M.; Tremolet de Villers, B. J.; Schulz, P.; Reese, M. O.; Ferrere, S.; Zhu, K.; Lin, L. Y.; Berry, J. J.; Luther, J. M. Influence of Electrode Interfaces on the Stability of Perovskite Solar Cells: Reduced Degradation Using MoOx/Al for Hole Collection. *ACS Energy Lett.* **2016**, *1* (1), 38–45. https://doi.org/10.1021/acsenergylett.6b00013.

(16) Dasgupta, B.; Goh, W. P.; Ooi, Z. E.; Wong, L. M.; Jiang, C. Y.; Ren, Y.; Tok, E. S.; Pan, J.; Zhang, J.; Chiam, S. Y. Enhanced Extraction Rates through Gap States of Molybdenum Oxide Anode Buffer. *J. Phys. Chem. C* **2013**, *117* (18), 9206–9211. https://doi.org/10.1021/jp3114013.

(17) Greiner, M. T.; Helander, M. G.; Tang, W.-M.; Wang, Z.-B.; Qiu, J.; Lu, Z.-H. Universal Energy-Level Alignment of Molecules on Metal Oxides. *Nat. Mater.* **2011**, *11*, 76.

(18) Kotadiya, N. B.; Lu, H.; Mondal, A.; Ie, Y.; Andrienko, D.; Blom, P. W. M.; Wetzelaer, G.-J. A. H. Publisher Correction: Universal Strategy for Ohmic Hole Injection into Organic Semiconductors with High Ionization Energies. *Nat. Mater.* **2018**, *17* (6), 563. https://doi.org/10.1038/s41563-018-0043-3.

(19) White, R. T.; Thibau, E. S.; Lu, Z.-H. Interface Structure of MoO3 on Organic Semiconductors. *Sci. Rep.* **2016**, *6*, 21109.

(20) Zapf, P. J.; Haushalter, R. C.; Zubieta, J. Hydrothermal Synthesis and Structural Characterization of a Series of One-Dimensional Organic/Inorganic Hybrid Materials of the [(MoO3)n(2,2′-Bipy)m] Family: [MoO3(2,2′-Bipy)], [Mo2O6(2,2′-Bipy)], and [Mo3O9(2,2′-Bipy)2]. *Chem. Mater.* **1997**, *9* (9), 2019–2024. https://doi.org/10.1021/cm970260o.

(21) Hagrman, P. J.; LaDuca Robert L.; Koo, H.-J.; Rarig Randy; Haushalter, R. C.; Whangbo, M.-H.; Zubieta, J. Ligand Influences on the Structures of Molybdenum Oxide Networks. *Inorg. Chem.* **2000**, *39* (19), 4311–4317. https://doi.org/10.1021/ic000496l.

(22) Vasilopoulou, M.; Douvas, A. M.; Georgiadou, D. G.; Palilis, L. C.; Kennou, S.; Sygellou, L.; Soultati, A.; Kostis, I.; Papadimitropoulos, G.; Davazoglou, D.; et al. The Influence of Hydrogenation and Oxygen Vacancies on Molybdenum Oxides Work Function and Gap States for Application in Organic Optoelectronics. *J. Am. Chem. Soc.* **2012**, *134* (39), 16178–16187. https://doi.org/10.1021/ja3026906.

Supporting Information. Kelvin probe and Contact angle measurements of the MoO_3 films with and without TPBi; and device data with alternative interfacial molecules are available in the Supporting Information. This material is available free of charge via the Internet at http://pubs.acs.org.

AUTHOR INFORMATION

Corresponding Author

* Authors to whom correspondence should be addressed: Pablo P. Boix (Pablo.P.Boix@uv.es) and Henk J. Bolink (henk.bolink@uv.es)

Author Contributions

All authors have given approval to the final version of the manuscript.

ACKNOWLEDGMENT

The authors would like to thank Alicia Forment for the contact angle measurements. Financial support is acknowledged from the Spanish Ministry of Economy and Competitiveness (MINECO) via the Unidad de Excelencia María de Maeztu MDM-2015-0538, MAT2017-88821-R, PCIN-2015-255, PCIN-2017-014 and the Generalitat Valenciana (Prometeo/2016/135). K.P.S.Z. acknowledges the financial support from Fundação de Amparo à Pesquisa do Estado de São Paulo (FAPESP

2018/05152-7). P.B and M.S. thanks the MINECO for their RyC contracts. P.B. acknowledges the financial support from the Conselleria d'Educació, Investigació, Cultura i Esport Valenciana (SEJI2017/2017/012).

TOC Graphic: